Chapter 0

Carbon Fibre Sensor: Theory and Application

Alexander Horoschenkoff and Christian Christner

Additional information is available at the end of the chapter

http://dx.doi.org/10.5772/50504

1. Introduction

The piezoresistive[1] carbon fibre sensor (CFS) consists of a single carbon fibre roving with electrical connected endings embedded in a sensor carrier (patch) for electrical insulation. Depending on the requirements of the application different patch types (e.g. glass fibre reinforced plastic (GFRP), polyester film, neat epoxy resin) are used. In terms of the mechanical properties GFRP is a particularly suitable patch material. CFSs with a GFRP patch exhibits an improved linearity of the signal due to the supportive effect of the glass fibres to the carbon sensor fibre especially in the case of compression loading. In [6] the ex-PAN fibre T300B was identified as one suitable carbon fibre for CFSs because of the excellent linear piezoresistive behaviour, the high specific resistivity and a high breaking elongation of the fibre. Figure 1 shows a CFS with a single layer GFRP patch (UD prepreg EG/913).

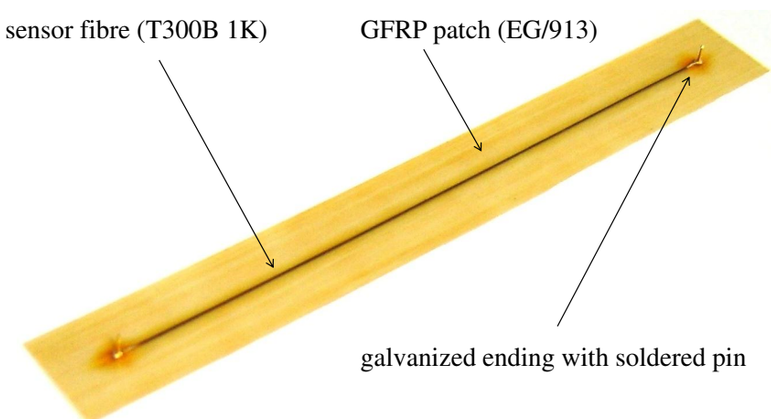

Figure 1. Carbon fibre sensor with an ex-Pan sensor fibre and a GFRP patch

[1] Piezoresitivity describes the change in electrical resistance of a conductor due to an applied strain.

The manufacturing process of a CFS includes three basic steps: Pre-curing of the carbon fibre, preparation of the electrical connection and embedding of the sensor fibre into the sensor carrier.

The pre-curing process is used to stabilize the carbon fibre roving and to align the filaments of the roving. For this purpose the twisted carbon fibre roving is impregnated by a resin with low viscosity and cured by using a special tooling. Good results for the impregnation of the carbon fibre roving T300B 1K were obtained by using the epoxy resin EP301 S (HBM) and a twist of 20 turns per meter. Spring elements provided a constant tension force along the roving during the curing process at 180 °C for 1.5 hours.

For preparation of electrical connections a galvanic process is applied based on a nickel electrolyte. In order to attain a homogeneous nickel coating of the filaments the resin must be removed at the fibre endings[2]. An applied current of 40 mA for 30 seconds leads to an excellent nickel coating. Depending on the application of the CFS (surface application or structural integration) the ends of the sensor fibre can be provided with soldered pins.

The embedding process of the sensor fibre depends on the used patch type and patch material. Figure 2 shows a micro section of a carbon fibre sensor in longitudinal and transverse direction.

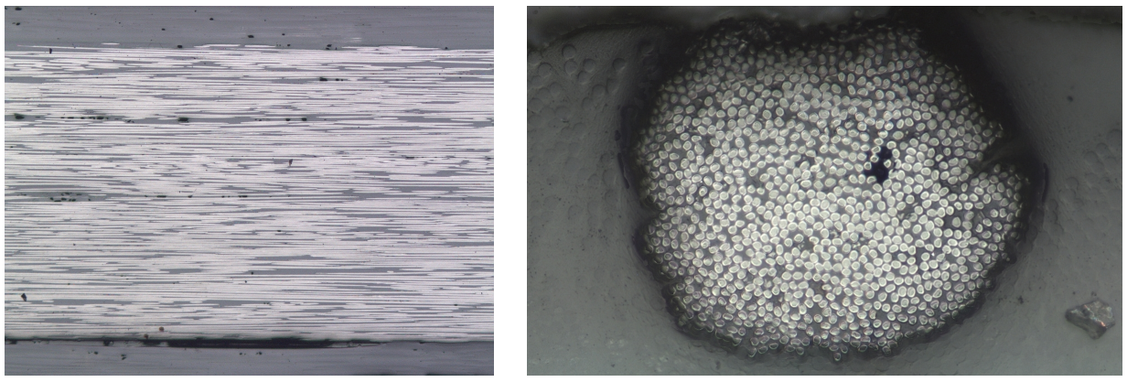

(a) Longitudinal direction (b) Transverse direction

Figure 2. Microsection of a carbon fibre sensor in longitudinal and transverse direction
Sensorfibre: 1K roving of the carbon fibre T300B
Patch: single layer UD prepreg EG/913

2. Electromechanical properties of carbon fibres

Referring to Chung [2] and Dresselhaus [3] crystalline carbon fibres have the same crystal structure as graphite. The layered and planar structure of crystalline carbon fibres is shown in Figure 3. In each layer the sp^2 hybridized carbon atoms are arranged in a hexagonal lattice. Within a layer (x-y plane) the carbon atoms are bonded by three covalent bonds (overlapping sp^2 orbitals), and a metallic bonding is provided by the delocalization of the p_z orbitals.

[2] For example, the epoxy resin EP 310 S can be burned off or removed using acid.

This delocalization of the fourth valence electron leads to a good electrical conductivity of the carbon fibre. The individual layers are held together by weak van der Waals forces (z-direction). These different types of bonds within and between the layers result in the anisotropy of the mechanical, thermal and electrical material properties of carbon fibres.

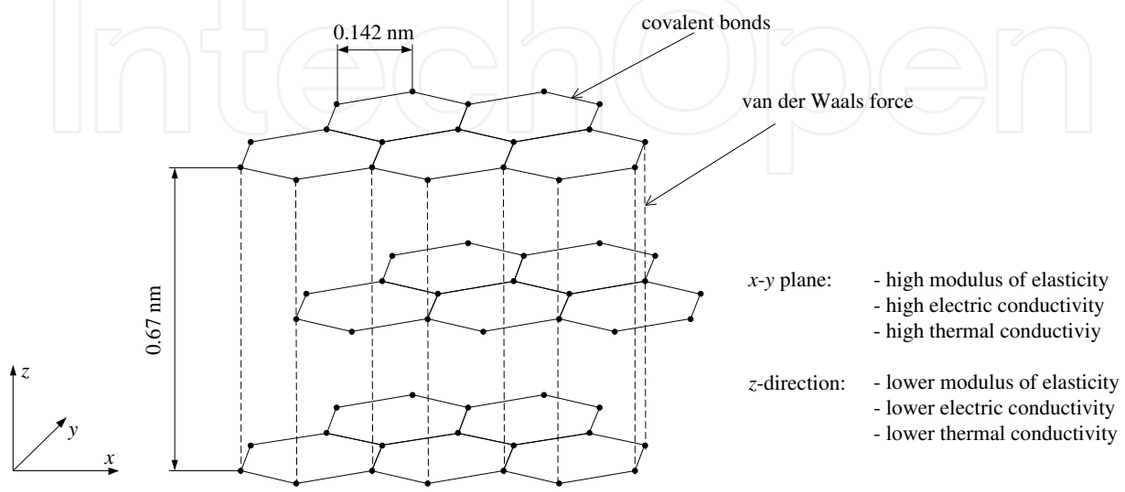

Figure 3. Graphite structure of crystalline carbon fibres

2.1. Specific resistivity

The degree of crystallinity and the micro structure of carbon fibres are controlled by the carbonisation process and determine the mechanical and electromechanical properties. Concerning ex-PAN fibres the Young's modulus ranges from 200 GPa (HT fibres) to 600 GPa (HM fibres). Ex-pitch fibres have a higher modulus up to 900 GPa. Figure 4 shows the correlation between the Young's modulus and the specific resistivity of different carbon fibre types. The specific resistivity of HT fibres (high tenacity) is in the range of 15 $\mu\Omega$m up to 18 $\mu\Omega$m. Higher orientated fibres (IM fibres and HM fibres) show a specific resistivity below 14 $\mu\Omega$m.

The specific resistance of carbon fibres is strongly temperature dependent [15]. In consequence, temperature effects have a high influence on the signals of CFSs and must be considered by an appropriate temperature compensation (see section 3).

2.2. Piezoresistivity

The electrical resistance R of a carbon fibre is given by:

$$R = \rho \frac{L}{r^2 \pi} \tag{1}$$

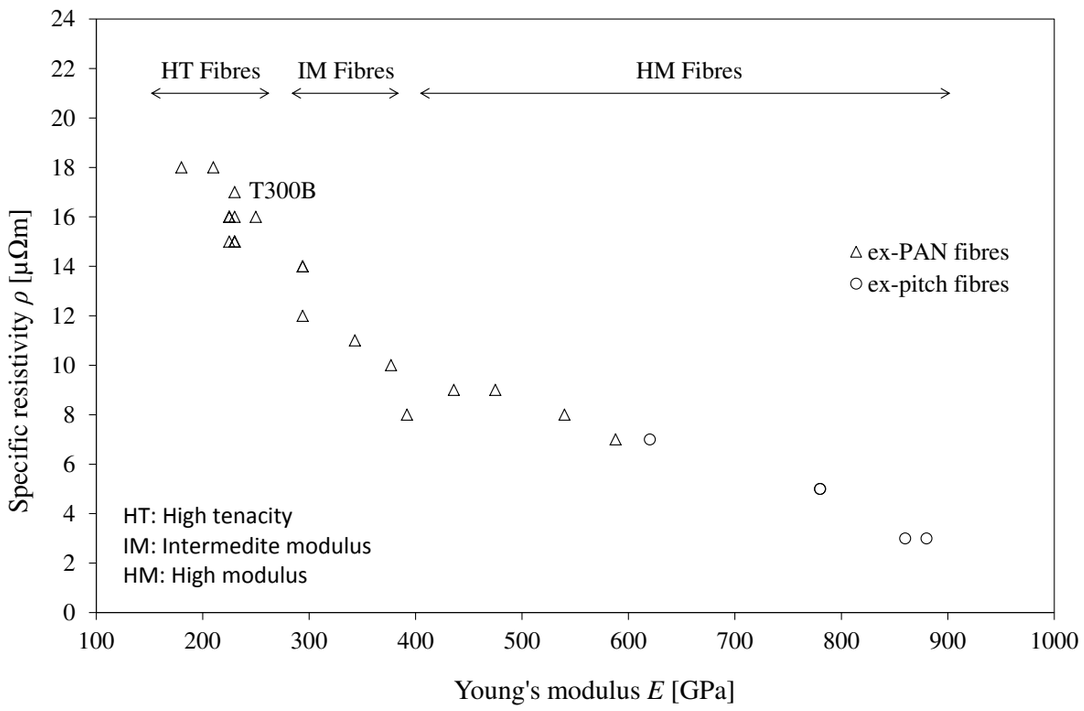

Figure 4. Correlation between the specific resistance ρ and the Young's modulus E of different ex-PAN and ex-pitch carbon fibres

where ρ is the specific resistivity, L the length and r the radius of the fibre. The total differential of $R = f(\rho, L, r)$ is then yielded by the following Equation (2).

$$\mathrm{d}R = \frac{\partial R}{\partial \rho}\mathrm{d}\rho + \frac{\partial R}{\partial L}\mathrm{d}L + \frac{\partial R}{\partial r}\mathrm{d}r = \frac{L}{r^2\pi}\mathrm{d}\rho + \rho\frac{1}{r^2\pi}\mathrm{d}L - 2\rho\frac{L}{r^3\pi}\mathrm{d}r \tag{2}$$

Using Equation (1) and Equation (2) the relative change in resistance of a carbon fibre $(\mathrm{d}R/R_0)$ can be expressed as:

$$\left(\frac{\mathrm{d}R}{R_0}\right) = \frac{\mathrm{d}\rho}{\rho} + \varepsilon(1+2\nu) = k\varepsilon \tag{3}$$

$$\text{with } \varepsilon = \frac{dL}{L} \text{ and } \nu = -\frac{dr/r}{dL/L}$$

The term $\mathrm{d}\rho/\rho$ denotes the piezoresistive effect (material effect) and the term $\varepsilon(1+2\nu)$ represents the geometric effects. The strain sensitivity k covers both effects. It should be noted that the strain sensitivity k depends on the effective Poisson ratio ν [3]. Therefore, the strain sensitivity k must be defined for a corresponding Poisson ratio[4].

[3] The effective Poisson ratio ν depends on the Poisson ratio of the sensor fibre ν_f, the Poisson ratio of the sensor patch ν_p and the strain ratio $-\varepsilon_y/\varepsilon_x$ of the structure.

[4] Conventional strain gauges exhibits the same behaviour. The strain sensitivity of strain gauges is usually defined for a corresponding Poisson ratio $\nu = 0.285$ (steel).

For some applications of CFSs it can be useful to split the strain sensitivity k into the longitudinal strain sensitivity k_l and the transverse strain sensitivity k_t. The relative change in resistance is then given by:

$$\left(\frac{\mathrm{d}R}{R}\right) = k_l \varepsilon_l + k_t \varepsilon_t \tag{4}$$

The strain sensitivity k of a T300B 1K fibre was determined as $k = 1.71$ for a corresponding Poisson ratio ν of 0.28. The sensor fibre exhibits a longitudinal strain sensitivity k_l in the range of 1.72 to 1.78 and a transverse strain sensitivity k_t in the range of 0.37 to 0.41. The piezoresistivity of the ex-PAN fibre is linear up to a strain level of approximately 6000 μm/m [1, 6]. Problems may occur at the metallized fibre endings. In order to avoid any influence of the electrical connections the strain level at the fibre endings should not exceed a level of 2500 μm/m.

This can be realized by using special tabs which exhibit a higher stiffness in the regions of the metallic connections. An example of such load relieving tabs is given in Figure 5. The lay-up of the tabs ensures a four times smaller strain level in the region of the electrical connections compared to the strain level which occurs in the testing area.

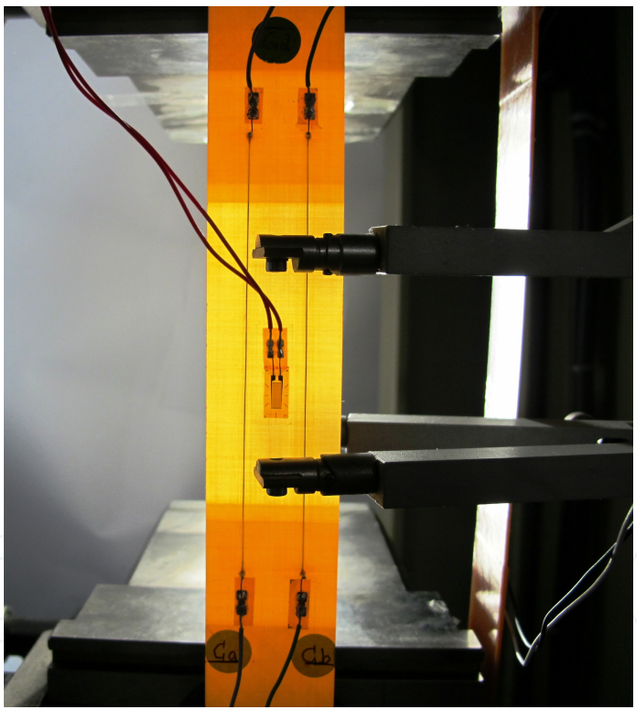

Figure 5. CFS patch with load relieving tabs
Lay-up in the testing area: $[0°]$
Lay-up in the regions of the metallized fibre endings: $[0_5^\circ]$

Figure 6 shows the excellent linear piezoresistive behaviour of the ex-PAN fibre T300B 1K up to a strain level of 6000 μm/m (loading and unloading). Bending tests were performed to investigate the compression behaviour of CFSs. These investigations are not completed. First results show that the linearity of the signal depends significant on the carrier material.

Ex-pitch fibres show a nonlinear piezoresistive behaviour.

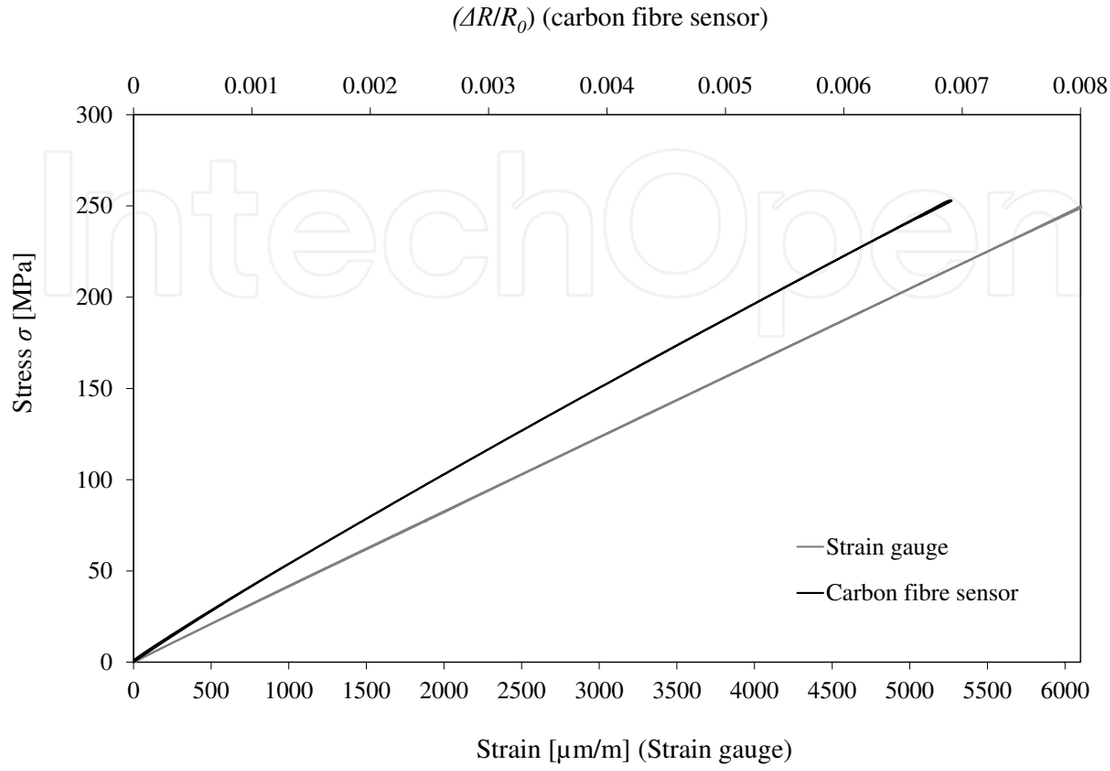

Figure 6. Characterization of the linear piezoresistivity up to a strain level of 6000 μm/m (loading and unloading) by means of a CFS patch with load relieving tabs at the endings
Sensor fibre: T300B 1K (ex-PAN fibre)
Lay-up in the testing area: $[0_8^\circ]$
Lay-up of the load relieving tabs: $[\pm 45^\circ, 0_3^\circ]_{sym}$

3. The Wheatstone bridge

The change in resistance of a CFS due to an applied strain is usually small. The Wheatstone bridge is an electrical circuit which allows the determination of very small changes in electrical resistance with great accuracy. Furthermore, the Wheatstone bridge minimizes the high influence of temperature changes on the CFS signal. The measurement circuit, illustrated in Figure 7, consists of four resistances, a supply voltage and the output voltage of the bridge. The relative change in resistance can be determined by the ratio of output voltage to input voltage V_{out}/V_s. There are two configurations of the Wheatstone bridge which are of special importance for the use of CFSs. These configurations of the Wheatstone bridge are known as "half bridge" configuration and "full bridge" configuration.

In the case of a half bridge circuit (Figure 8(a)), the bridge is formed by two CFSs (R_1 and R_2) and two completion resistors (R_3 and R_4). The full bridge configuration (Figure 8(b)) is formed by four CFSs and needs no additional resistors. Both circuits will enable a compensation of

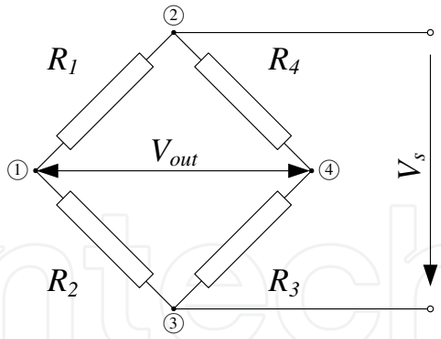

$R_1 \ldots R_4$: resistances, bridge arms
V_s: bridge supply voltage
V_{out}: bridge output voltage

$$\frac{V_{out}}{V_s} = \frac{1}{4}\left(\frac{\Delta R_1}{R_1} - \frac{\Delta R_2}{R_2} + \frac{\Delta R_3}{R_3} - \frac{\Delta R_4}{R_4}\right)$$

Figure 7. General Wheatstone bridge circuit

temperature effects (thermal dependency of the specific resistance and thermal expansion) if the thermal conditions of the connected CFSs are identical. In the case of a half bridge circuit with one active CFS (R_1) the output voltage V_{out} is given by:

$$V_{out} = \frac{V_s}{4}\left(\frac{\Delta R_{1,mech} + \Delta R_{1,therm}}{R_1} - \frac{\Delta R_{2,therm}}{R_2}\right) \tag{5}$$

Equation (5) shows that the thermal effect is compensated by the mechanically unloaded carbon fibre sensor (R_2). Detailed information about the principle and use of the Wheatstone bridge can be found in classical textbooks on strain gauge techniques (e.g. [5, 13])

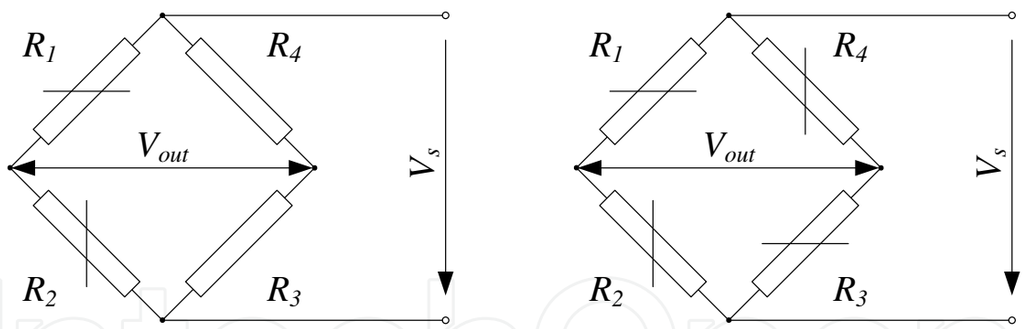

(a) Half bridge circuit (b) Full bridge circuit

Figure 8. Half bridge and full bridge configuration of the Wheatstone bridge

4. Integral strain measurement of the carbon fibre sensor

Equation (3) describes the relative change in electrical resistance $(\Delta R/R_0)$ of a carbon fibre sensor due to an applied elastic strain ε. It is important to understand that a CFS measures the strain integrally along its whole fibre length. Thus, Equation (3) can be written as:

$$\left(\frac{\Delta R}{R_0}\right) = k\frac{1}{L}\int_0^L \varepsilon(x)\,\mathrm{d}x \tag{6}$$

Equation (6) shows that a CFS measures the displacement between the terminal points of the sensor fibre.

$$\left(\frac{\Delta R}{R_0}\right)\frac{L}{k} = \int_0^L \varepsilon(x)\,\mathrm{d}x = [u(x=L) - u(x=0)] \tag{7}$$

This integral strain measurement of CFSs in accordance to Equation (7) can be used to create carbon fibre sensor meshes (CFS meshes). Such a CFS mesh allows the determination of the two dimensional (2D) state of strain and state of deformation of a whole structure or larger areas of a structure.

5. Carbon fibre sensor meshes

The strain and deformation analysis by means of CFS meshes are based on linear or higher order displacement approximations. The displacement functions depend on the used element type such as 3-node triangle elements, 6-node triangle elements or quadrilateral elements. The basic theory of strain analysis with CFS meshes using 3-node triangle elements with a linear displacement approximation is presented below.

A triangular CFS element defined by its vertices 1, 2, 3 and its local coordinate system is given in Figure 9.

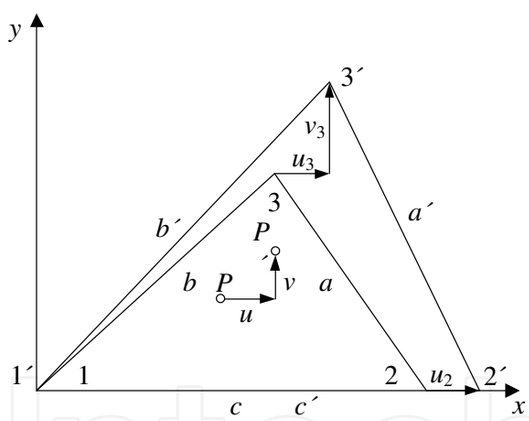

(a) Definition local coordinate system

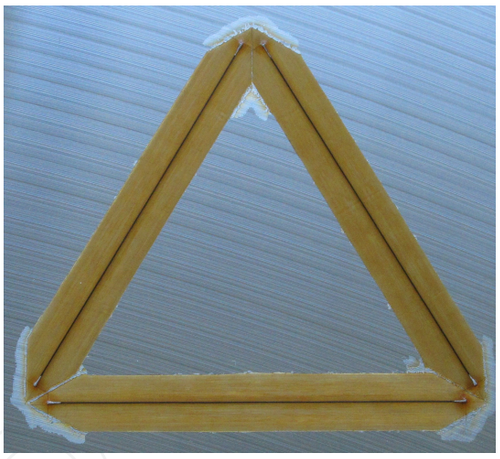

(b) CFS element applied on aluminium

Figure 9. Triangle CFS element with 3 nodes

The displacement $u(x,y)$ and $v(x,y)$ of an inner point P can be determined by the displacements of the vertex in using a displacement function.

Assuming a linear displacement function the displacement $u(x,y)$ and $v(x,y)$ within the element can be calculated in accordance to Equation (8) and Equation (9).

$$u(x,y) = N_1u_1 + N_2u_2 + N_3u_3 \tag{8}$$

$$v(x,y) = N_1v_1 + N_2v_2 + N_3v_3 \tag{9}$$

Hereby u_i and v_i denote the displacements of the vertex 1, 2, 3 in the x- and y-direction while N_i represents the shape functions of the element. The shape functions N_i of a 3-node

triangle can be found in classical books on the theory of finite element analysis (e.g. [16]). The engineering strains ε_x, ε_y and γ_{xy} are defined by:

$$\varepsilon_x = \frac{\delta u}{\delta x}; \qquad \varepsilon_y = \frac{\delta v}{\delta y}; \qquad \gamma_{xy} = \frac{\delta u}{\delta y} + \frac{\delta v}{\delta x} \tag{10}$$

Considering the local coordinate system ($u_1 = 0, v_1 = 0, v_2 = 0$) the strains within the triangle can be calculated by:

$$\varepsilon_x = \frac{u_2}{x_2}; \qquad \varepsilon_y = \frac{v_3}{y_3}; \qquad \gamma_{xy} = \frac{x_2 u_3 - x_3 u_2}{x_2 y_3} \tag{11}$$

In consequence of the linear displacement approximation the strains are independent of the coordinates (x and y) and thus constant within the element. The unknown displacements u_2, u_3 and v_3 of the vertex 2 and 3 can be determined by the signals of the carbon fibre sensors.

In order to verify this linear approach an experimental investigation of a CFS mesh applied on a 1000 mm x 1000 mm x 5 mm PMMA plate was performed. The simply supported plate was loaded with a single static force at the center. In addition to the experiment a finite element analysis (FEA) was performed. In [9] the results of this experiment and of the corresponding finite element simulations are presented in detail [5]. Figure 10 shows the PMMA plate and the applied CFS mesh.

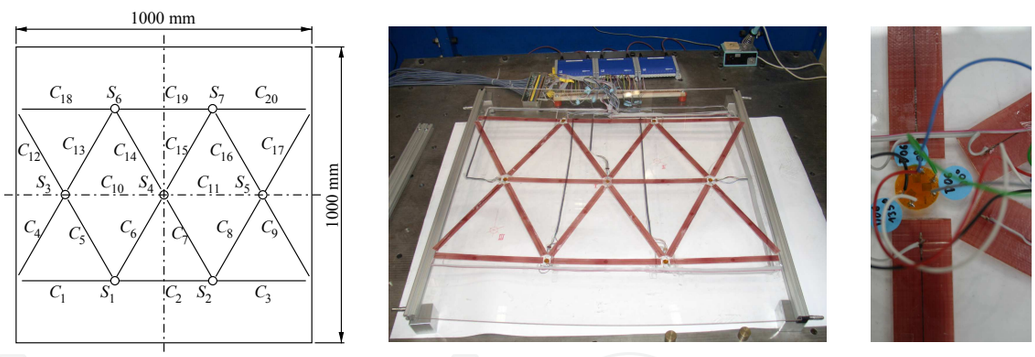

Figure 10. Carbon fibre sensor mesh applied on a 1 m x 1 m PMMA plate. Each sensor has a length of 300mm. [9]

Figure 11 shows the determined strain ε_x for each element of the mesh. There was a good correlation between the measured and the calculated strain levels. The accuracy was in the range of $\pm$ 5%.

The results of the performed investigation show that CFS meshes are a reliable instrument to determine the strain fields and principle strains of lightweight structures.
The principle strains (strain level and direction) are of particular interest in case of structures made of composite materials. For example, tailored fibre placement (TFP) is an advanced textile manufacturing process for CFRP structures in which the carbon fibre rovings are placed

[5] A quadratic displacement approach for a 3-node triangle is also presented and verified in [9]. However, the quadratic displacement approach of a 3-node triangle requires additional strain gauges at the nodes to determine the 12 unknown coefficients of the shape function.

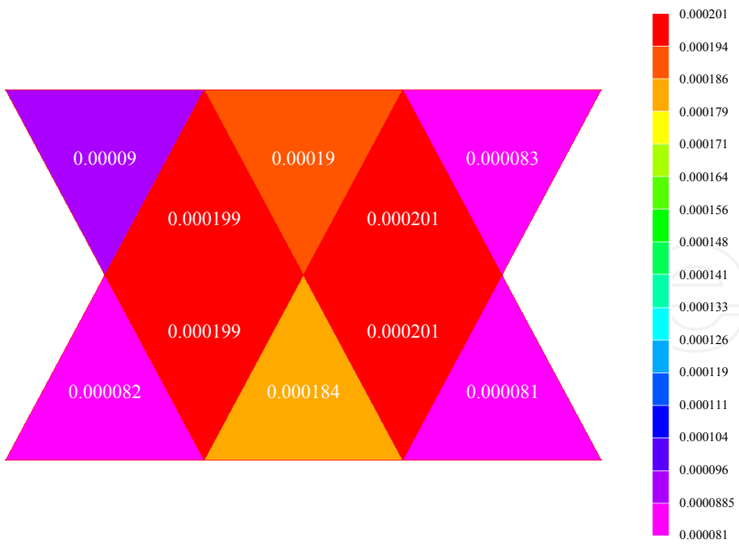

Figure 11. Strain ε_x measured by the carbon fibre sensor mesh

in accordance to the direction of principal stresses.
The finite element simulation is a powerful tool to analyse the stress fields and principle directions of lightweight structures. At the design and optimization processes the FEA is almost the only way to evaluate the structural load. However, there is a lack of techniques to review the results of the FEA. CFS meshes offer a high potential to verify the results of the finite element analysis.

6. Micro crack detection

A major failure mode of multidirectional reinforced laminates is transverse matrix cracking. Matrix cracks will reduce the effective stiffness of the laminate and will result in local stress concentrations at the crack tip. Furthermore, interlaminar crack growth and local delamination can occur. Due to its integral strain measurement method the CFS has a high potential to detect matrix crack initiation and monitor crack growth. Figure 12 shows a thin GFRP laminate (Lay-up: $[90^\circ_2, 0^\circ, 90^\circ_2]$) which has two embedded CFSs. Matrix cracks along the CFS will affect the sensor signal which will give a clear indication of the crack density. A study was performed to investigate the influence of cracks on the sensor signal [10]. The study was performed on the GFRP laminate $[0^\circ, 90^\circ_5, 0^\circ, 90^\circ_5, 0^\circ]$. Three CFSs were embedded in the mid-plane 0°-layer. At a strain level higher than 3000 μm/m matrix cracks appeared in the 90°-layers. The following techniques were applied to characterize the influence of damages on the sensor signal:

- Acoustic emission analysis in combination with pattern recognition technique
- Microscopy and micrographs
- Analytical calculations
- Finite element analysis

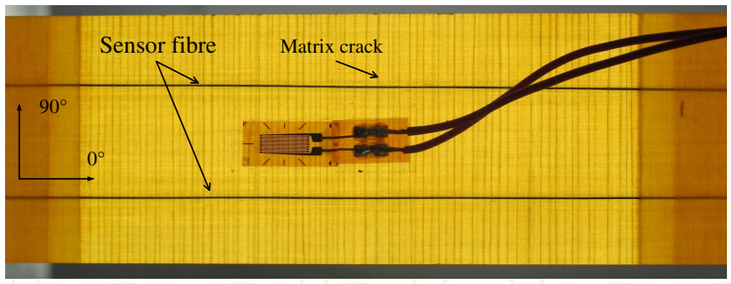

Figure 12. Multidirectional reinforced GFRP laminate with two embedded CFSs. Transverse matrix cracking will affect the sensor signal.
Lay-up: $[90_2^\circ, 0^\circ, 90_2^\circ]$

Figure 13 shows the correlation between the crack density, the CFS signals, the acoustic emission energy (AE-energy), the strain level measured by a strain gauge and the according stress level. It can be seen that the matrix crack initiation causes first AE-signals and a change of the slope of the CFS signals.

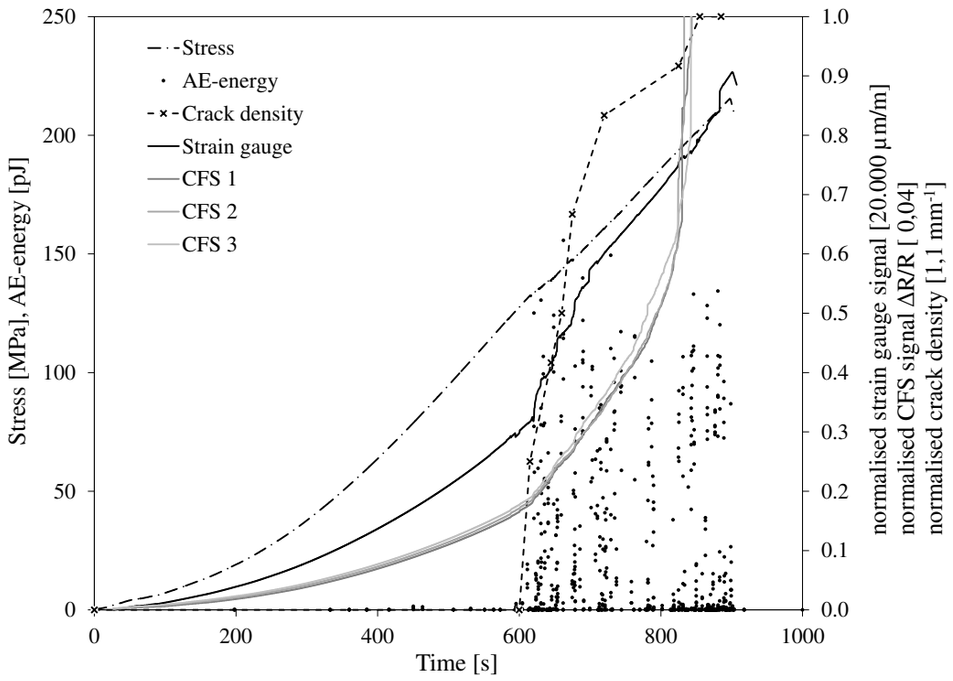

Figure 13. Acoustic emission and CFS signals measured on an GFRP laminate under uniaxial tensile load [10]
Lay-up: $[0^\circ, 90_5^\circ, 0^\circ, 90_5^\circ, 0^\circ]$

Furthermore, a good correlation between the sensor signal $(\Delta R/R_0)$ and the crack density can be observed. After having reached a crack density of 0.8 mm^{-1} the signals of the embedded carbon fibre sensors increase disproportionately. The analytical approach of Garret and Bailey [4, 11, 12] and a FEA were applied to calculate the reduction of the stiffness of the laminate. Müller showed that the global stiffness loss of the laminate due to the matrix cracking can be measured by means of the CFS. However, at high strain levels ($>$ 70% of $\varepsilon_{ultimate}$) there

is a strong influence of high local stresses at the crack tip on the CFS signal. These stress concentrations may result in filament breakage and in extremely high signal levels.

Based on this result CFSs can be used for damage monitoring and for the prediction of the lifetime of damaged structures if the damage level can be characterized by stiffness loss. Figure 14 shows the cyclic loading of a laminate to measure the stiffness loss and to determine Ladeveze's material parameters [8]. Based on this calibration the lifetime of a structure, e.g. pressure vessel, can be predicted.

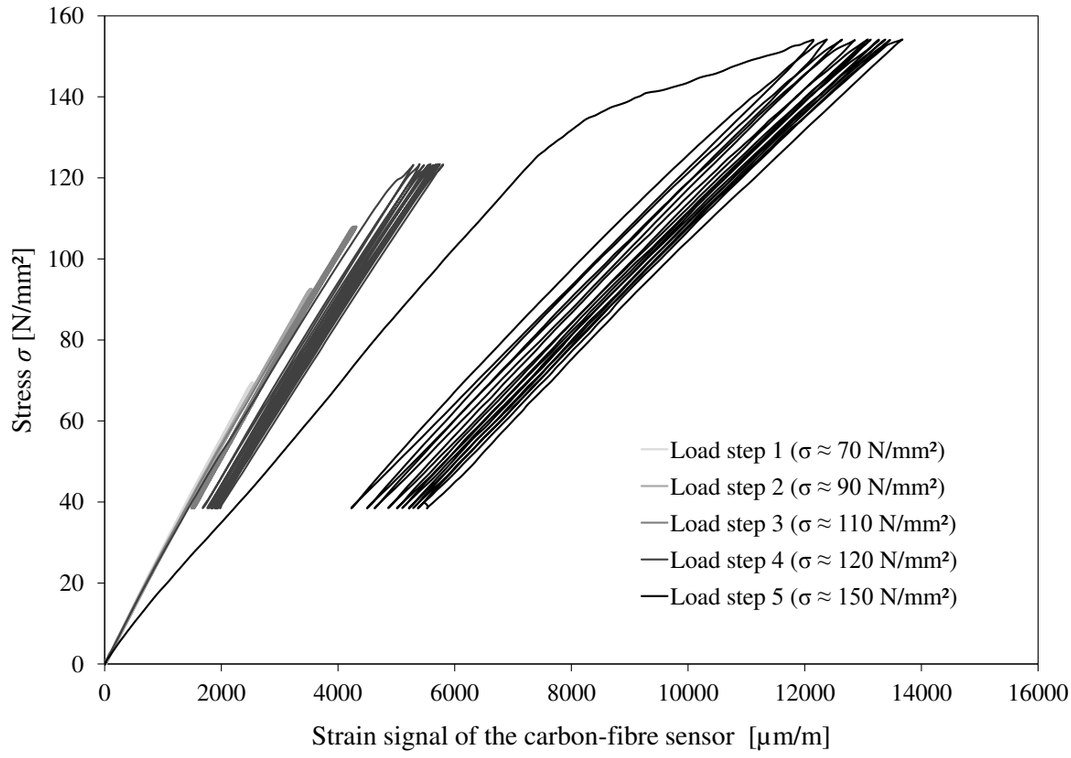

Figure 14. Damage measurement and determination of damage variables like the energy release rate
Material: GFRP, EG/913
Lay-up: $[0°, 90°_5, 0°, 90°_5, 0°]$

7. Impact and delamination detection

An impact loading can cause small damages inside the composite material which may not be found by visible inspection. One major concern is delamination damages or the disbonding of interfaces. These damages result in sublaminates having lower buckling resistance and compression strength. Although a small delamination-damage does not necessarily constitute failure, the damaged area may undergo a time-dependent growth and may attend a critical size.

The principles for achieving damage tolerant primary composite structures were established by the aircraft companies [14]. Maintenance intervals and inspection plans are determined in

such a way that readily detectable damages will be repaired before damage growth can affect the fatigue strength of the structure. The influence of undetectable damages is covered by the so called barely visible impact damage (BVID) which defines the damage that establishes the strength values to be used in analysis to demonstrate compliance with the load requirements. One method to determine the influence of the BVID on the mechanical performance is the compression after impact test procedure (CAI-test procedure, i.e. Boeing BSS 7260). A 4 mm thick quasi-isotropic test specimen (150 x 100 mm) is damaged by a dropped weight impact testing machine. An impact level of about 3 J/mm will cause the BVID. This means that only a small remaining indentation is visible on the surface of the specimen, but delamination may be found inside. The strength of the damaged specimen is reduced by 10 to 20% compared to the undamaged material. This shows that in many cases the exploitation of material performance is limited, since the skin thicknesses of a composite structure are designed to absorb an impact.

For aircraft structures health monitoring systems have an extremely high potential to improve the efficiency of composite structures. Based on a monitoring system the material design values can be increased and the inspection intervals can be enlarged. Both aspects can result in a weight reduction of the structure up to 10%. A preliminary study was performed to investigate the use of CFSs as a sensor system to detect the BVID. The CAI specimen was used to integrate a rectangular CFS mesh (Figure 15 and Figure 16).

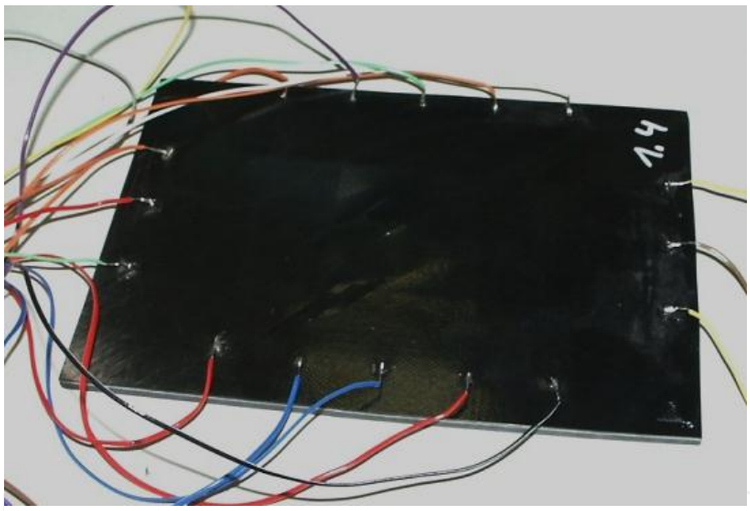

Figure 15. Compression after impact (CAI)-specimen with integrated CFS mesh to detect damages below the barely visible impact damage level (BVID)

The distance between the CFSs varied from 30 to 100 mm. Three methods were investigated to detect the impact damage:

- Online measurements of the resistivity during the impact test
- Offline measurements, comparison of the resistivity before and after the impact
- Active thermography, CFSs used as heating element

It has been shown that all three procedures are suitable to detect impact damages. A distance of 50 mm between the CFSs is necessary to detect even small damages below the

BVID. In a second step the use of CFSs will be investigated to detect debonding of skin and stringer. A health monitoring system for a complex aircraft structure will be based on several technologies like ultrasonic inspection sensors and strain sensors. The CFS technology will complement the established sensors due to its specific and simple integral measurement principle.

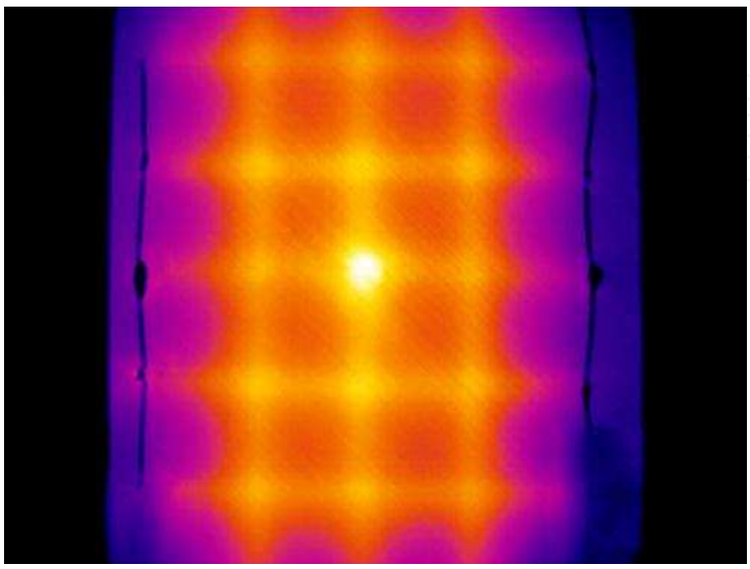

Figure 16. Compression after impact (CAI)-specimen with integrated CFS mesh. The CFSs are used as heating element for active thermography. A small delamination damage is visible (BVID)

8. Application

CFSs offer a high potential to be used as a sensor element for composite materials for stress analysis, damage detection and the monitoring of manufacturing processes. Two industrial applications have been selected to demonstrate this.

8.1. Tabletop of a CT-Scanner

Carbon fibre reinforced plastics (CFRP) are used for tabletops of computer tomography (CT) scanners, since CFRP fulfills the X-Ray transparency which is necessary to get the picture quality sufficient for medical diagnosis.

CFSs can be embedded in the tabletop of a CT scanner to measure its deflection. Based on the measured deflection the CT images can be readjusted to result in an improved medical attendance [7]. Figure 17 shows the tabletop of a CT scanner with ten u-shaped CFSs applied. For this application u-shaped CFSs are used to avoid that any metal wiring is part of the scan plane for all operation positions. The lengths of the u-shaped CFSs vary from 250 to 1250 mm. The determination of the beam deflection is based on the integral strain measurement of CFSs (Equation (6)). Considering small deformations the relation between the elastic strain of the outer fibre $\widehat{\varepsilon}$ and the beam deflection v is given by:

$$v = \iint v'' \mathrm{d}x\mathrm{d}x = \iint \frac{\widehat{\varepsilon}}{e_y} \mathrm{d}x\mathrm{d}x \tag{12}$$

Figure 17. CT tabletop with u-shaped CFSs to measure the deflection. The metallic wiring is attached to the clamping support.

where e_y denotes the distance from the neutral axis. Assuming a cantilever beam (see Figure 18) the slope v' of the beam can be determined directly by the signals of the CFSs. Assuming that the CFS starts at the clamping support ($x = 0$) the slope v' at the end of the applied CFS ($x = l_i$) becomes:

$$v'(x = l_i) = \frac{l_i}{k e_y} \left(\frac{\Delta R}{R} \right)_i \tag{13}$$

The deflection y of the beam can be calculated by numerical integration.

$$v(x = l_i) = \sum_{n=1}^{i} \left[v'(x_n) - \frac{v'(x_n) - v'(x_{n-1})}{2} \right] (l_n - l_{n-1}) \tag{14}$$

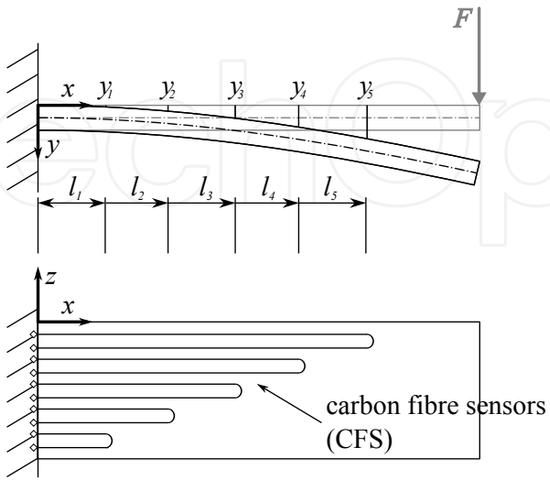

Figure 18. Side and top view of a cantilever beam with five u-shaped CFS

The index i denotes the number of CFSs applied. The quality of the approximation in accordance to Equation (14) depends on the complexity of the loading, the number of applied CFSs and the used sensor configuration.

In the case of the CT table (Figure 17) the deflection of the table can be determined with an accuracy of ± 0.3 mm for different operation positions. Figure 19 shows a typical measurement. The operating position of the CT tabletop varies stepwise from 0 mm to 2000 mm and back to 0 mm. The weight of the used dummy is 100 kg and electrical half bridges are used for temperature compensation.

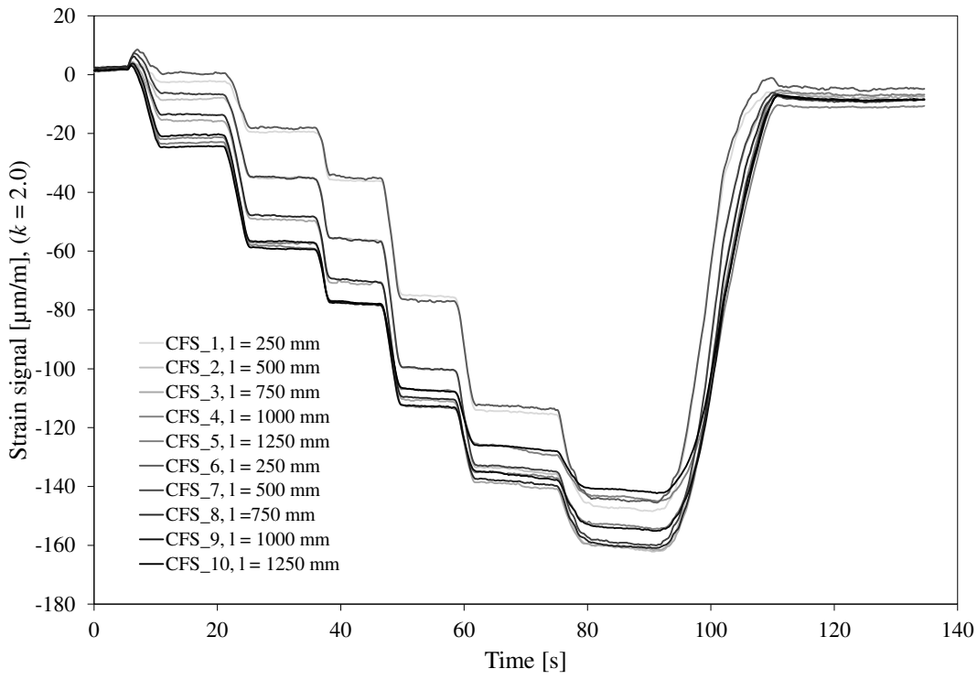

Figure 19. CFS signals of the CT table for a weight of 100 kg and different operation positions, ranging from 0 to 2000 mm

8.2. Pressure vessels

For thin walled assumptions the longitudinal stress σ_l and hoop stress σ_r in the cylindrical portion of a pressure vessel, away from the ends, are given by:

$$\sigma_l = \frac{pr}{2t} \tag{15}$$

$$\sigma_r = \frac{pr}{t} \tag{16}$$

where t is the thickness and r is the radius of the vessel. The relation σ_r/σ_l shows that the efficiency of pressure vessels can be increased if hoop wrapped vessels are used. A metal cylinder is reinforced by carbon fibres having a radial orientation (type II vessels). The strength of the vessel is increased remarkably.

There are two aspects for the use of CFSs for pressure vessels which can be easily integrated by means of the winding process:

- Determination of the pressure level of the vessel
- Monitoring of degradation processes due to fatigue or overloading of the radial fibre reinforcement

For such an application a sensor patch with four CFSs connected in full-bridge configuration is particularly suitable, since the full-bridge circuit minimizes the influences of thermal effects and shows an improved long term stability of the signal. Figure 20 shows such a hoop wrapped vessel with an embedded CFS patch.

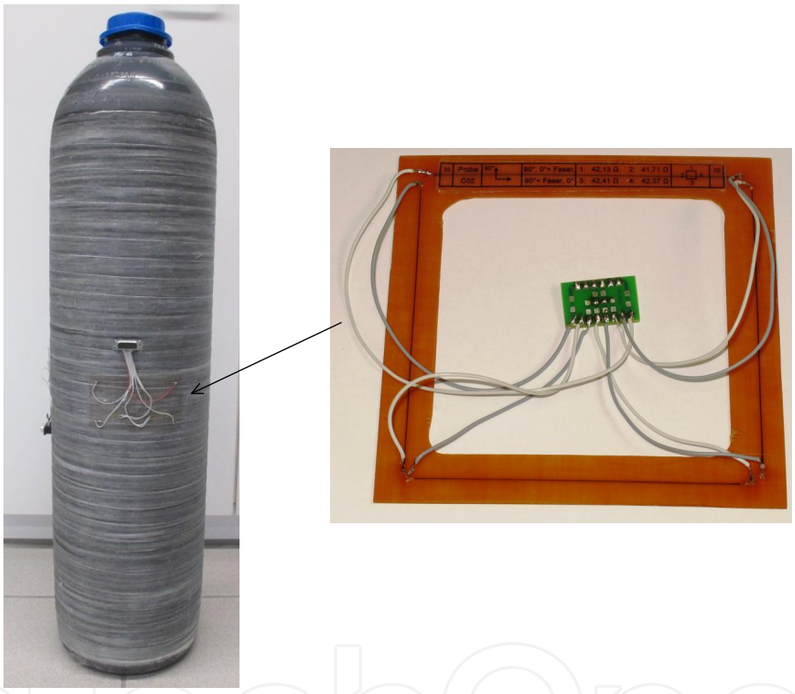

Figure 20. Hoop wrapped pressure vessel (type II vessel) with embedded CFSs

Experimental studies showed that the pressure of the vessel can be determined by using a CFS patch with a resolution of about 1 bar. A representative measurement of the performed test is shown in Figure 21. The pressure load of the vessel was increased stepwise up to a maximum pressure level of 100 bar. The subsequent pressure relief was performed in the same manner.

Micro cracks in the CFRP layers of the pressure vessel may occur as a result of mechanical or thermal overloading. The failure of the matrix causes a loss of stiffness of the CFRP layers and reduces the global stiffness of the vessel. Depending on the crack density and the crack growth the lifetime of the structure will decrease. Based on the damage master curve of the structure, an estimation of the remaining lifetime can be performed (see Figure 14).

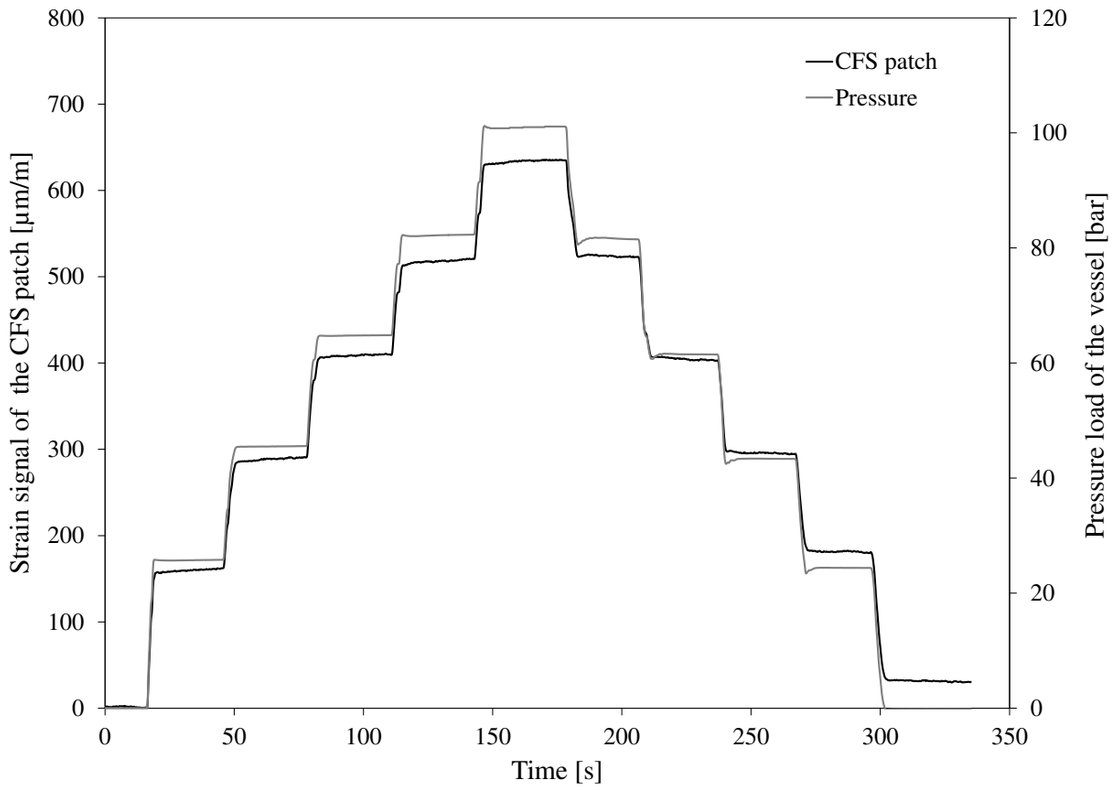

Figure 21. Strain signals of a CFS patch applied near the surface of a type II pressure vessel subjected to a pressure test

9. Conclusion

There are three main aspects which made carbon fibre sensors (CFSs) very interesting to be used for composite materials:

- Material-conformity
- Linear piezoresistivity up to high strain levels
- Integral strain measurement method

CFSs based on a T300B 1K ex-Pan fibre exhibit an excellent linear piezoresistivity up to a strain level of 6000 μm/m. The according strain sensitivity was determined as $k = 1.71$ (related to a Possion ratio of $\nu = 0.28$). The longitudinal strain sensitivity k_l of the CFS is in the range of 1.72 - 1.78. Transverse to the fibre direction CFSs exhibit a transverse strain sensitivity k_t of approximately 0.4. This significant transverse strain sensitivity must be considered in praxis. Tension load was applied for all tests, the characterization of the compression behaviour is under examination.

A disadvantage of CFSs is the high influence of temperature on the signal which will be an aspect for future research. At the moment a long term stability of ± 2 μm/m ($T = const.$) can be achieved for a half or full bridge circuit.

CFSs can be used for strain analysis, damage monitoring and the control of manufacturing processes. Concerning strain and stress analysis an approach for CFS meshes was developed based on triangular elements with linear displacement approximation. A good correlation was found between the measurement and the finite element calculation. The use of CFS meshes can be a new approach to complement finite element analysis from the experimental side.

Concerning monitoring aspects the influence of material damages on the sensor signal were studied. It has been demonstrated that based on the integral strain measurement method the CFS is an excellent sensor to detect delaminations and matrix cracks in multidirectional reinforced laminates. Therefore, the CFS offers unique features for fracture mechanics: Measurement of strain levels and detection of matrix cracks. By means of two examples the CFS technologies could be demonstrated successfully:

- Determination of the deflection of a tabletop of a CT-Scanner
- Determination of the strain level and the crack density of a pressure vessel

Strain measurement and matrix crack detection are in the focus of safe and damage tolerant composite structures making the CFS technology a complement of established sensors.

Author details

Alexander Horoschenkoff
Munich University of Applied Sciences, Germany

Christian Christner
Universität der Bundeswehr München, Germany

10. References

[1] Christner, C., Horoschenkoff, A. & Rapp, H. [2012]. Longitudinal and transverse strain sensitivity of embedded carbon-fibre sensors, *Journal of Composite Materials* Online First: DOI: 10.1177/0021998312437983.
[2] Chung, D. [1994]. *Carbon Fiber Composites*, Butterworth-Heinemann.
[3] Dresselhaus, M., Dresselhaus, G., Sugihara, K., Spain, I. & Goldberg, H. [1988]. *Graphite Fibers and Filaments*, Springer.
[4] Garrett, K. & Bailey, J. [1977]. Multiple transverse fracture in 90° cross-ply laminates of a glass fibre-reinforced polyester, *Journal of Material Science* Vol. 12: 157–168.
[5] Hoffmann, K. [1987]. *An introduction to measurements using strain gages*, Hottinger Baldwin Messtechnik.
[6] Horoschenkoff, A., Müller, T. & Kröll, A. [2009]. On the charaterization of the piezoresistivity of embedded carbon fibres, *17th International Conference on Composite Materials*, Edinburgh.
[7] Horoschenkoff, A., Müller, T., Strössner, C. & Farmbauer, K. [2011]. Use of carbon-fibre sensors to determine the deflection of composite-beams, *18th International Conference on Composite Materials*, International Conference on Composite Materials, Jeju.

[8] Ladeveze, P. & Dantec, E. L. [1992]. Damage modelling of the elementary ply for laminated composites, *Composite Science and Technology* Vol. 43: 257–267.
[9] Matzies, T., Christner, C., Müller, T., Horoschenkoff, A. & Rapp, H. [2011]. Carbon-fibre sensor meshes: Simulation and experiment, *21st International Workshop on Computational Mechanics of Materials*, Limerick.
[10] Müller, T., Horoschenkoff, A., Rapp, H., Sause, M. & Horn, S. [2010]. Einfluss von zwischenfaserbrüchen in 0/90-laminaten auf die elektrische widerstandsänderung von eingebetteten carbonfasern, *59th Deutscher Luft- und Raumfahrkongress*.
[11] Nairn, J. [1989]. The strain energy relase rate of composite microcracking: A variational approach, *Journal of Composite Materials* Vol. 23: 1106–1129.
[12] Nairn, J. & Hu, S. [1994]. Matrix microcracking, *Damage Mechanics of Composite Materials* Vol. 9: 187–243.
[13] Perry, C. & Lissner, H. [1955]. *The Strain Gauge Primer*, Mc Gram Hill.
[14] Razi, H. & Ward, S. [1996]. Principles for achieving damage tolerant primary composite aircraft structures, *11th DoD/FAA/NASA Conference on Fibrous Composites in Structural Design*.
[15] Spain, I., K., V., Goldberg, H. & Kalnin, I. [1982]. Unusual electrical resistivity behavior of carbon fibres, *Solid State Communications* Vol. 45(No.): 817–819.
[16] Zienkiewicz, O. & Taylor, R. [2000]. *Finite Element Method Volume 1: The Basis*, Elsevier.